

Direct Competition between hnRNP C and U2AF65 Protects the Transcriptome from the Exonization of *Alu* Elements

Kathi Zarnack,^{1,8} Julian König,^{2,8} Mojca Tajnik,^{2,3} Iñigo Martincorena,¹ Sebastian Estermann,² Isabelle Stévant,¹ Alejandro Reyes,⁴ Simon Anders,⁴ Nicholas M. Luscombe,^{1,5,6,7,*} and Jernej Ule^{2,*}

¹European Molecular Biology Laboratory (EMBL) European Bioinformatics Institute, Wellcome Trust Genome Campus, Hinxton, Cambridge CB10 1SD, UK

²MRC Laboratory of Molecular Biology, Hills Road, Cambridge CB2 0QH, UK

³Faculty of Medicine, University of Ljubljana, Vrazov trg 2, SI-1104 Ljubljana, Slovenia

⁴EMBL, Genome Biology Unit, Meyerhofstraße 1, 69117 Heidelberg, Germany

⁵UCL Genetics Institute, Department of Genetics, Environment and Evolution, University College London, Gower Street, London WC1E 6BT, UK

⁶Cancer Research UK London Research Institute, 44 Lincoln's Inn Fields, London WC2A 3LY, UK

⁷Okinawa Institute for Science and Technology Graduate University, 1919-1 Tancha, Onna-son, Kunigami-gun, Okinawa 904-0495, Japan

⁸These authors contributed equally to this work

*Correspondence: nicholas.luscombe@ucl.ac.uk (N.M.L.), jule@mrc-lmb.cam.ac.uk (J.U.)

<http://dx.doi.org/10.1016/j.cell.2012.12.023>

SUMMARY

There are ~650,000 *Alu* elements in transcribed regions of the human genome. These elements contain cryptic splice sites, so they are in constant danger of aberrant incorporation into mature transcripts. Despite posing a major threat to transcriptome integrity, little is known about the molecular mechanisms preventing their inclusion. Here, we present a mechanism for protecting the human transcriptome from the aberrant exonization of transposable elements. Quantitative iCLIP data show that the RNA-binding protein hnRNP C competes with the splicing factor U2AF65 at many genuine and cryptic splice sites. Loss of hnRNP C leads to formation of previously suppressed *Alu* exons, which severely disrupt transcript function. Minigene experiments explain disease-associated mutations in *Alu* elements that hamper hnRNP C binding. Thus, by preventing U2AF65 binding to *Alu* elements, hnRNP C plays a critical role as a genome-wide sentinel protecting the transcriptome. The findings have important implications for human evolution and disease.

INTRODUCTION

Most eukaryotic primary transcripts consist of short exons and very long introns. This exon-intron structure provides important opportunities for proteome diversity and evolution. The selective usage of exons through alternative splicing is a major source of proteome diversity in higher organisms (Nilsen and Graveley, 2010). Furthermore, the long intronic regions facilitate the

creation of new protein functionalities through exon shuffling by nonallelic recombination between different genes (Fedorova and Fedorov, 2003; Xing and Lee, 2006).

The complex gene structure means that nascent transcripts must be carefully processed before they can be used. In particular, the precise removal of introns in the splicing reaction demands the complex interplay between a multitude of *trans-acting* factors and *cis*-regulatory splicing signals in the pre-messenger RNA (pre-mRNA) molecule. Among the former, a multisubunit complex called the spliceosome catalyzes intron excision and exon joining at splice sites (Wahl et al., 2009). Among the latter, the GU and AG dinucleotides, flanked by additional sequence elements, define intron-exon boundaries at the 5' and 3' splice sites. The most prominent flanking element is a sequence rich in uridines and cytidines, known as the polypyrimidine tract, which is located immediately upstream of the 3' splice site, and is required for binding of the U2 auxiliary factor 65 (U2AF65). Binding of U2AF65 is essential for recruiting the small nuclear ribonucleoprotein (snRNP) U2, a component of the spliceosome, and thus comprises a major regulatory event during 3' splice-site recognition (Wahl et al., 2009).

Although the splicing reaction is carried out with very high precision, the *cis*-acting signals that mediate spliceosome binding show limited sequence constraint. As a result, pre-mRNAs harbor a large number of potential splice sites with very similar sequences to true splice sites, but that are not used under normal conditions. Importantly, these cryptic splice sites can act as a source of new exons during evolution. On the other hand, uncontrolled recognition of cryptic splice sites can have deleterious consequences for the cell if it creates aberrant transcripts, and the inclusion of cryptic exons has been implicated in various diseases (Buratti et al., 2007; Dhir and Buratti, 2010; Vorechovský, 2006). It is therefore imperative for the cell to tightly control the accessibility of such signals to the splicing machinery.

Candidates for masking cryptic splice sites are the heterogeneous nuclear ribonucleoproteins C1/C2 (referred to as hnRNP C). hnRNP C is abundant in the nucleus and associates with all nascent transcripts (Beyer et al., 1977; König et al., 2010). It forms hnRNP particles, which have been described to compact large regions of pre-mRNA and have been implicated in the regulation of alternative splicing (Choi et al., 1986; Dreyfuss et al., 1993). In order to investigate the function of hnRNP C on a genomic scale, we previously developed a technique called individual-nucleotide resolution UV-crosslinking and immunoprecipitation (iCLIP) (König et al., 2010, 2011). Using iCLIP, we characterized the transcriptome-wide binding pattern of hnRNP C at an unprecedented resolution and discovered that hnRNP C represses alternative exons by binding next to the splice sites (König et al., 2010). However, the mechanism by which this repression is achieved, and its importance in repressing cryptic exons, remained unclear.

Here, we introduce iCLIP as a high-resolution, quantitative technique that enables us to measure how the competition between hnRNP C and the core splicing factor U2AF65 regulates the inclusion of alternative exons on a genomic scale. Notably, we show that hnRNP C blocks U2AF65 from cryptic 3' splice sites, thereby preventing the aberrant expression of cryptic exons. Finally, we dissect how the differences in sequence specificities of hnRNP C and U2AF65 enable the splicing machinery to discriminate cryptic splice sites from genuine exons, and reveal the importance of hnRNP C for maintaining transcriptome integrity and preventing disease.

RESULTS

hnRNP C and U2AF65 Bind at 3' Splice Sites

To investigate the detailed molecular function of hnRNP C, we first explored the potential for iCLIP to provide quantitative measurements of protein-RNA interactions. With an optimized protocol, we identified a total of 14 million unique hnRNP C crosslink events in untreated HeLa cells, which cluster into 438,360 binding sites (Table S1 and Figure S1A available online). This represents a 22-fold increase in crosslink events compared with our previously published data (König et al., 2010). The greatly increased complexity of the new data set allowed us to rank binding sites by their normalized occupancy, and to estimate the strength of hnRNP C-RNA associations. We find that the strongest binding sites reside at continuous uridine tracts (U-tracts) of nine or more uridines (Figure S1B, bottom). Overall, hnRNP C binds to more than 10% of all U-tracts of nine or more uridines in the human transcriptome, underlining the importance of U-tract length in determining hnRNP C binding to pre-mRNAs (Figure S1B, top).

hnRNP C shows widespread binding across introns (Figures 1 and S1A). In addition to this broad pattern, the protein shows specific binding to the polypyrimidine tracts of alternative exons that it represses (Figure S1C; repressed exons determined from RNA-sequencing [RNA-seq] data, see below). To explore the effects of this binding, we performed iCLIP experiments with the splicing factor U2AF65 that associates with polypyrimidine tracts to enable exon inclusion (Figures S2A and S2B). This yielded a total of 12 million crosslink events, corresponding to

518,794 binding sites (Table S1). The replicate data sets revealed very consistent binding locations and normalized occupancies within each site, indicating the high reproducibility of the quantitative information contained within the iCLIP data (Figure S3A).

In contrast to the extended binding pattern of hnRNP C, U2AF65 displays more restricted binding, with a strong preference for the regions directly upstream of 3' splice sites (Figures 1, S1A, and S1D). We detect U2AF65 binding at 58% of all actively used 3' splice sites in HeLa cells, underlining its crucial role in splice-site recognition. Intriguingly, U2AF65 binding at the 3' splice sites of all exons (Figure S1D) coincides with the peak of hnRNP C binding at repressed exons (Figure S1C), suggesting that the two proteins might compete for pre-mRNA binding.

hnRNP C Competes with U2AF65 Binding

To assess competition between hnRNP C and U2AF65, we performed U2AF65 iCLIP experiments in *HNRNPC* knockdown HeLa cells (Figures S2A and S2B). Independent *HNRNPC* knockdowns with two different siRNAs affected neither U2AF65 protein levels nor the protein's general ability to bind RNA (Figures S2A and S2C). The experiments in the knockdown cells produced 15 million highly reproducible crosslink events; combined with the data from the control samples, this yielded a total of 1.1 million U2AF65-binding sites (Table S1). To compare differences in U2AF65 binding between conditions, we corrected for changes in transcript levels by normalizing the numbers of crosslink events. The changes in U2AF65 binding in the two independent *HNRNPC* knockdowns were highly correlated, allowing us to combine both data sets for the remaining analyses (referred to as KD; $r = 0.545$, Pearson's product-moment correlation; Figure S3B).

Loss of hnRNP C has a dramatic impact on U2AF65 binding: thousands of sites display increased U2AF65 occupancy, with over 3,000 sites showing at least 4-fold increases (Figure S3C). Importantly, these changes are largest at sites that directly overlap with hnRNP C binding (p value $< 10^{-16}$, Student's *t* test; Figure 2A), suggesting that U2AF65 gains access to sites that are normally occupied by hnRNP C. In particular, 1,698 (51%) of the ~3,000 most upregulated sites coincide with an hnRNP-C-binding site (Figure 2B; p value $< 10^{-15}$ compared with unchanged sites, Fisher's exact test). Significantly, the changes in U2AF65 occupancies increase with the strength of hnRNP C binding (Figure 2A), in line with the characteristics of competitive binding. Moreover, only 4% or 7% of binding sites with decreased or unchanged U2AF65 occupancy coincide with hnRNP C binding, respectively. These results indicate that hnRNP C blocks U2AF65 from a large number of binding sites in the transcriptome.

A number of hnRNP proteins, including hnRNP H (Heiner et al., 2010), PTB (hnRNP I; Saulière et al., 2006), and hnRNP A1 (Tavanez et al., 2012), have previously been described to compete with, or proofread, U2AF65 binding. To test whether these and other RNA-binding proteins function together with hnRNP C, we examined published binding data for seven hnRNP proteins (hnRNP A1, A2B1, F, H, M, U, and PTB; Huelga et al., 2012; Xue et al., 2009). We also included TIA1, TIAL, and TDP-43, which recognize U-rich motifs (Tollervey et al., 2011;

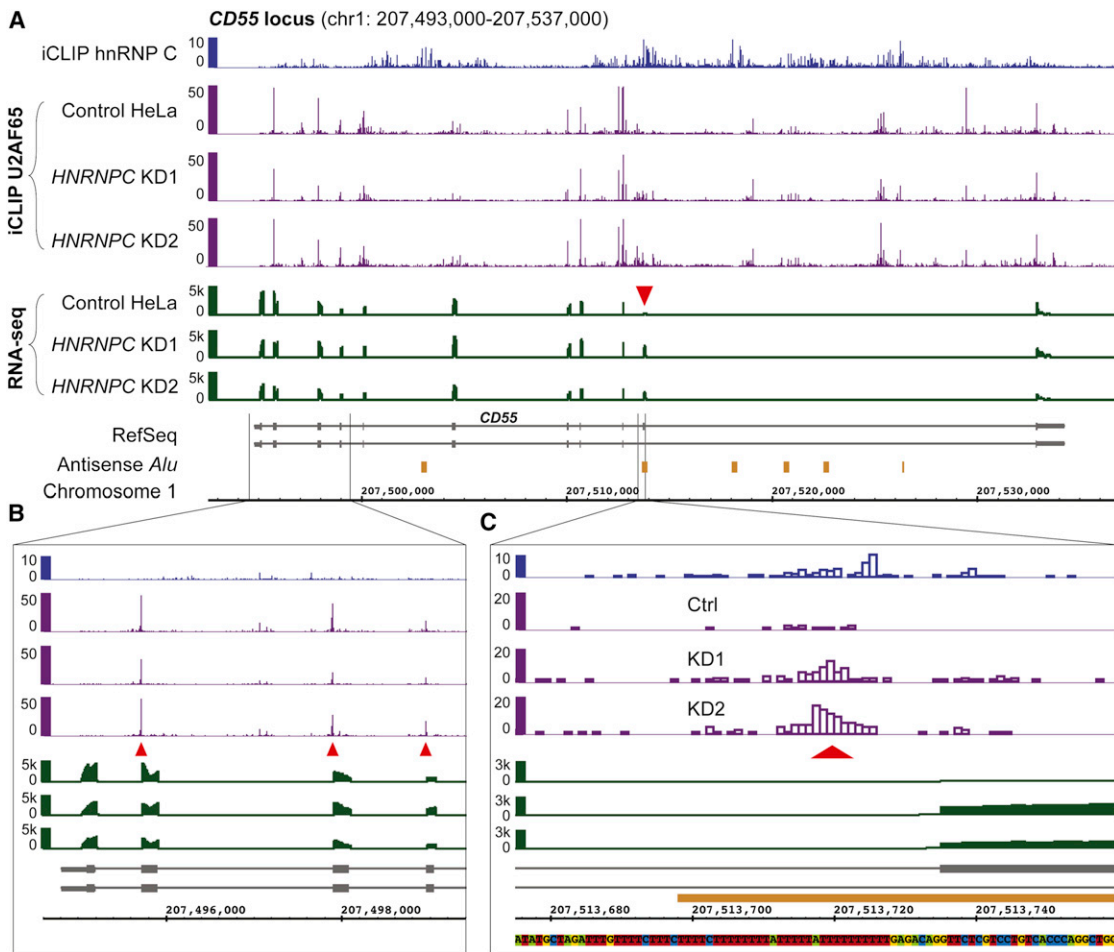


Figure 1. Examples of U2AF65 and hnRNP C Binding at the 3' Splice Sites of Constitutive or hnRNP-C-Repressed Exons within the CD55 Gene

(A) Genome browser view of the *CD55* gene displaying the iCLIP data (crosslink events per nucleotide) of hnRNP C (blue) and U2AF65 (purple) as well as the RNA-seq data (overlapping reads per nucleotide; green) from control and *HNRNPK* knockdown HeLa cells. The red arrowhead marks the hnRNP-C-repressed alternative *Alu* exon. RefSeq transcript annotations (gray) and *Alu* elements in antisense orientation to the shown strand (orange) are depicted below.

(B) Enlargement of the genomic region containing the 5' UTR and the first four exons. Red arrowheads mark U2AF65 peaks at 3' splice sites.

(C) Enlargement of the region around the 3' splice site of the hnRNP-C-repressed *Alu* exon (marked in A) including the underlying genomic sequence. The red arrowhead marks the site of increased U2AF65 occupancy in the *HNRNPKD1* knockdown.

See also Figures S1 and S2.

Wang et al., 2010). TIA1, TIAL, TDP-43, and PTB, but none of the other proteins, display noticeable crosslinking at loci containing both U2AF65 and hnRNP C binding (Figure 2C). We tested whether their presence affects competitive binding by assessing the changes in U2AF65 occupancies in the *HNRNPK* knockdown. As expected, most of the increase in U2AF65 binding (at sites overlapping with hnRNP C) can be explained by the loss of hnRNP C alone (84%; Figure 2D). Sites additionally containing TIA1, TIAL, or TDP-43 binding show a slightly bigger increase. In contrast, sites overlapping with PTB show a reduced shift (Figure 2D), suggesting that PTB and hnRNP C might act redundantly. However, because we observe these combinatorial effects only at a minor fraction of sites (16% of all shared U2AF65-hnRNP-C-binding sites; Figure 2E), we conclude that hnRNP C alone is sufficient to compete with U2AF65 in the majority of cases.

A key feature of the competition between hnRNP C and U2AF65 is their overlapping, but differing, sequence specificity: both proteins bind uridines, but U2AF65 can also recognize cytidines (Figure 2F; Görlich et al., 1994; König et al., 2010; Norton, 1994; Singh et al., 2000; Swanson and Dreyfuss, 1988). A comparison of pentameric sequences within binding sites shows that U2AF65 associates with diverse uridine- and cytidine-containing pentamers, contrasting hnRNP C's selective preference for continuous uridines (Figures 2G and S3D). In the *HNRNPK* knockdown, we observe a specific increase in U2AF65 binding only to the uridine pentamer (Figure 2G), indicating that U-tracts that are otherwise protected by hnRNP C become accessible. Consistently, the biggest changes in U2AF65 binding occur at long U-tracts (Figure S3E). These observations suggest that the competition between the two proteins occurs at a specific subset of U2AF65-binding sites,

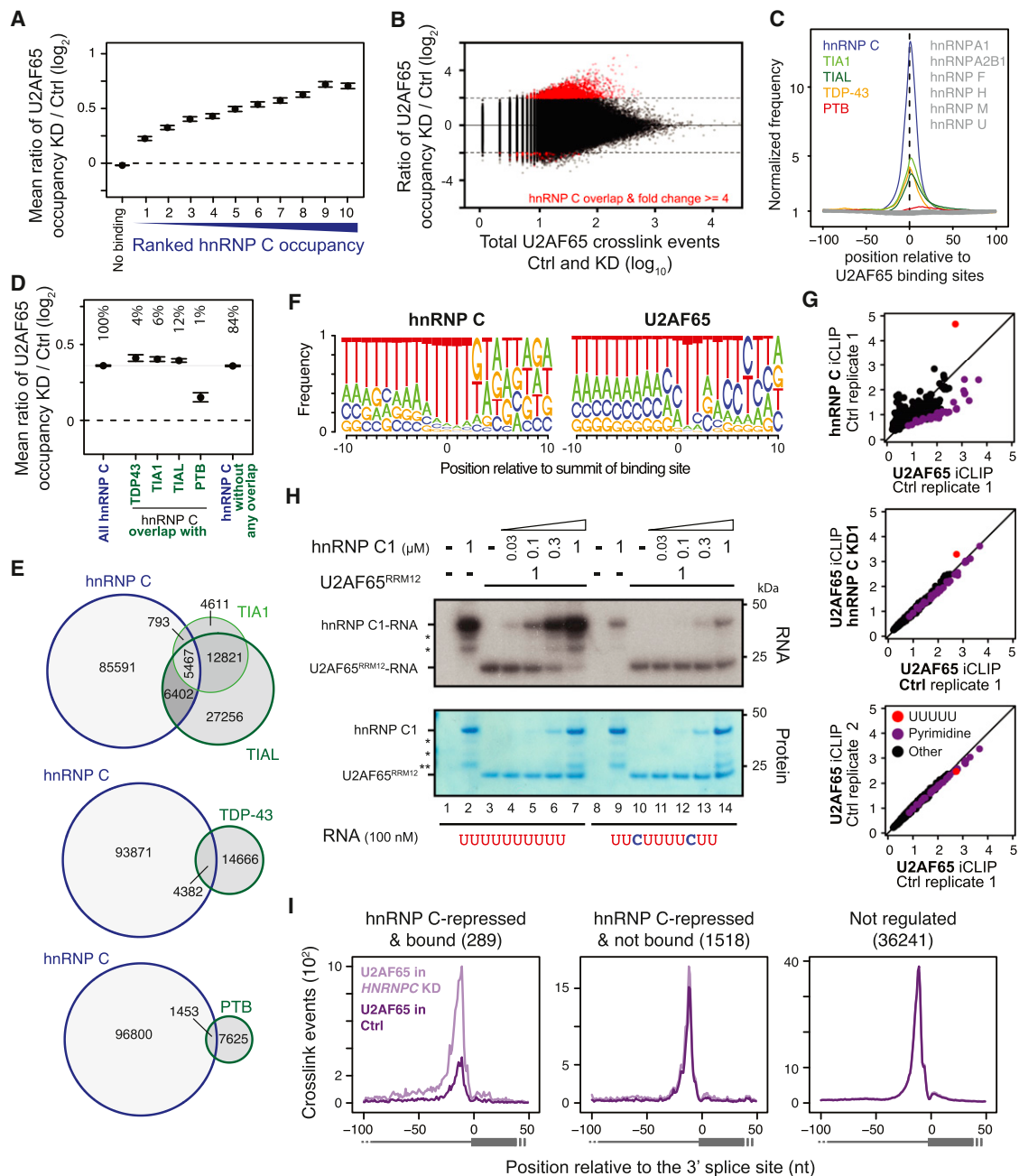


Figure 2. hnRNP C and U2AF65 Compete for Binding on U-Tracts and at Regulated Exons

(A) The average ratio of U2AF65 occupancies from knockdown (KD) over control is shown for U2AF65-binding sites that do not overlap with hnRNP C (no binding) or that overlap with hnRNP-C-binding sites within different ranks of hnRNP C occupancy (i.e., rank 10 contains the 10% strongest hnRNP-C-binding sites). Error bars indicate the 95% confidence interval of the mean.

(B) Plot showing the ratio of U2AF65 occupancies against the total number of U2AF65 crosslink events for individual binding sites. Binding sites that show an at least 4-fold change in occupancy and overlap with hnRNP C binding are depicted in red.

(C) Plots depicting the frequency of overlapping binding sites of ten other RNA-binding proteins around the summit of U2AF65-binding sites (position 0) that overlap with hnRNP C. Proteins that show increased crosslinking are colored.

(D) Plot as in (A) showing U2AF65-binding sites that overlap with hnRNP C compared to sites that overlap with both hnRNP C and TIA1, TIAL, TDP-43, or PTB (indicated below) and sites that overlap with only hnRNP C and none of the other proteins. The percentage of shared hnRNP-C-U2AF65-binding sites within the different categories is indicated above.

(E) Weighted Venn diagrams depicting the overlap of U2AF65-binding sites that are bound by hnRNP C (blue) and/or either TIA1/TIAL, TDP-43, or PTB (green). Absolute numbers are given within each segment.

(F) Weblogos showing the relative nucleotide frequency around the summits (position 0) of hnRNP-C- and U2AF65-binding sites.

(legend continued on next page)

namely at long U-tracts, which constitute prime hnRNP-C-binding sites.

hnRNP C Blocks U2AF65 from Continuous U-Tracts In Vitro

To test whether the competition is direct, we performed in vitro UV-crosslinking assays (Warf et al., 2009). For this, we used a recombinant full-length hnRNP C1 protein and a fragment of U2AF65 containing the first two RRM domains (U2AF65^{RRM12}), which was previously shown to retain the binding characteristics of the full-length protein (Mackereth et al., 2011). We first tested the binding of both proteins individually to two RNA oligonucleotides, resembling a high-affinity hnRNP-C-binding site (U₁₀), as well as a modified version carrying two cytidines at positions 3 and 8. Whereas U2AF65^{RRM12} shows comparable binding to both RNAs, hnRNP C1 binding is drastically impaired by the two interspersed cytidines (Figures S3G and S3H), in line with the divergent sequence preferences of the two proteins.

We next assessed the direct competition between both proteins by adding increasing concentrations of hnRNP C1 to the U2AF65^{RRM12}-binding reaction. U2AF65^{RRM12} binding to the U₁₀ RNA decreases with increasing amounts of hnRNP C1 and is almost completely abolished at equimolar concentrations (Figure 2H). Conversely, U2AF65^{RRM12} binding to the cytidine-containing RNA remains largely unaffected in the presence of hnRNP C1. These results demonstrate that hnRNP C alone is sufficient to displace U2AF65 from continuous U-tracts. Notably, this competition is alleviated by interspersed cytidines, allowing strong U2AF65 binding in the presence of hnRNP C.

The hnRNP C-U2AF65 Competition Leads to Exon Repression

Our iCLIP and in vitro binding data demonstrate that hnRNP C blocks U2AF65 from a large number of binding sites. To investigate how this competition influences splicing, we performed RNA-seq experiments using the same two *HNRNPC* knockdowns as well as control HeLa cells (Table S1). We first monitored changes in gene expression using the DESeq software, identifying 4,880 and 4,875 genes that showed significant differential expression in KD1 and KD2, respectively (adjusted p value < 0.01). Using Cufflinks, we then determined transcript structures de novo to detect all expressed exons in the knockdown and control samples (Trapnell et al., 2010). We identified changes in splicing patterns using the DEXSeq software (Anders et al., 2012) and observed a good correlation in splicing

changes between both knockdowns; this indicates that the changes arise as a consequence of hnRNP C depletion rather than off-target effects of the siRNAs used ($r = 0.567$, Pearson's product-moment correlation; Figure S4A). By combining the knockdown data sets, we obtained a high-confidence set of 3,052 differentially expressed exons, including 1,807 and 1,245 that are repressed and enhanced by hnRNP C, respectively (Table S2; Figure S4B).

A total of 289 (16%) repressed exons harbor an hnRNP-C-binding site less than 30 nucleotides upstream of their 3' splice site (14-fold enrichment compared with all other exons; p value < 10⁻¹⁵, Fisher's exact test), compared with only 1%–2% of enhanced or unchanged exons. Using an RNA map depicting changes in U2AF65 binding, we find a clear 3-fold increase in U2AF65 occupancy upon *HNRNPC* knockdown at exons that are bound and repressed by hnRNP C (Figure 2I). In dramatic contrast, exons that are either not regulated or not bound by hnRNP C display no change in U2AF65 binding (Figure 2I). We conclude that competition with U2AF65 constitutes the mechanism of hnRNP-C-mediated repression of exons with proximal hnRNP C binding, whereas the remaining exons might be regulated via distal hnRNP-C-binding sites or other effects that do not alter U2AF65 binding. An example of a competitive event at the 3' splice site can be seen at the alternative exon of the *CD55* gene: *HNRNPC* knockdown leads to a strong increase in U2AF65 binding, accompanied by significantly elevated exon inclusion (Figure 1C). In summary, these observations indicate that hnRNP C represses alternative exons by directly interfering with U2AF65 recognition.

hnRNP C Prevents the Aberrant Exonization of *Alu* Elements

The observations so far have explained the function of hnRNP C at known alternative exons; however, it is clear that the vast majority of hnRNP C binding occurs at “deep” intronic regions without exon annotations (Figure S1A). Strikingly, we find that hnRNP C binding in these regions also blocks U2AF65 activity: in fact, 75% of the U2AF65-binding sites that display strongest competition with hnRNP C are located more than 200 nucleotides away from any Ensembl-annotated exon (Figure S3F), suggesting that hnRNP C prevents recognition of cryptic splicing signals. This is confirmed in the RNA-seq data, which show that 41% of hnRNP-C-repressed exons do not overlap with existing annotations in the Ensembl database (Table S2). This indicates that hnRNP C prevents the aberrant inclusion of cryptic exons that are normally excluded from transcripts.

(G) Plots comparing the pentamer fold-enrichment around crosslink sites from replicate experiments with hnRNP C and U2AF65 from control and *HNRNPC* knockdown HeLa cells. The three panels compare iCLIP data from (i) experiments with both proteins from untreated HeLa cells (Ctrl; left), (ii) replicate experiments with U2AF65 from Ctrl cells (middle; see also Figure S3D), and (iii) experiments with U2AF65 from *HNRNPC* knockdown (KD1) and Ctrl cells (right).

(H) Autoradiograph from an in vitro UV crosslinking assay using recombinant hnRNP C1 (33 kDa) and U2AF65^{RRM12} proteins (21 kDa). A stable amount of U2AF65^{RRM12} plus increasing concentrations of hnRNP C1 (indicated above in μ M) were UV crosslinked to radioactively labeled wild-type (U₁₀, lanes 1–7) and mutant (U₂CU₄CU₂, lanes 8–14) RNA oligonucleotides (100 nM) and analyzed by denaturing gel electrophoresis. Radioactive signals of RNA crosslinked to hnRNP C1 or U2AF65^{RRM12} are marked on the left. Asterisks indicate C-terminal hnRNP C1 truncations (*) and GST (*). Coomassie staining of the same gel (bottom) serves as loading control. Note that there is an additional hnRNP C1 signal likely representing an hnRNP C1 dimer, which is only shown in Figure S3H.

(I) RNA maps showing the total number of crosslink events of U2AF65 in control HeLa (light purple) and *HNRNPC* knockdown cells (dark purple) relative to the 3' splice sites of all exons that (i) are repressed and bound by hnRNP C (left), (ii) are repressed but not bound by hnRNP C (middle), and (iii) are not subject to any regulation in the *HNRNPC* knockdown (fold change < 1.1; right). The number of exons in each category is indicated above.

See also Figure S3.

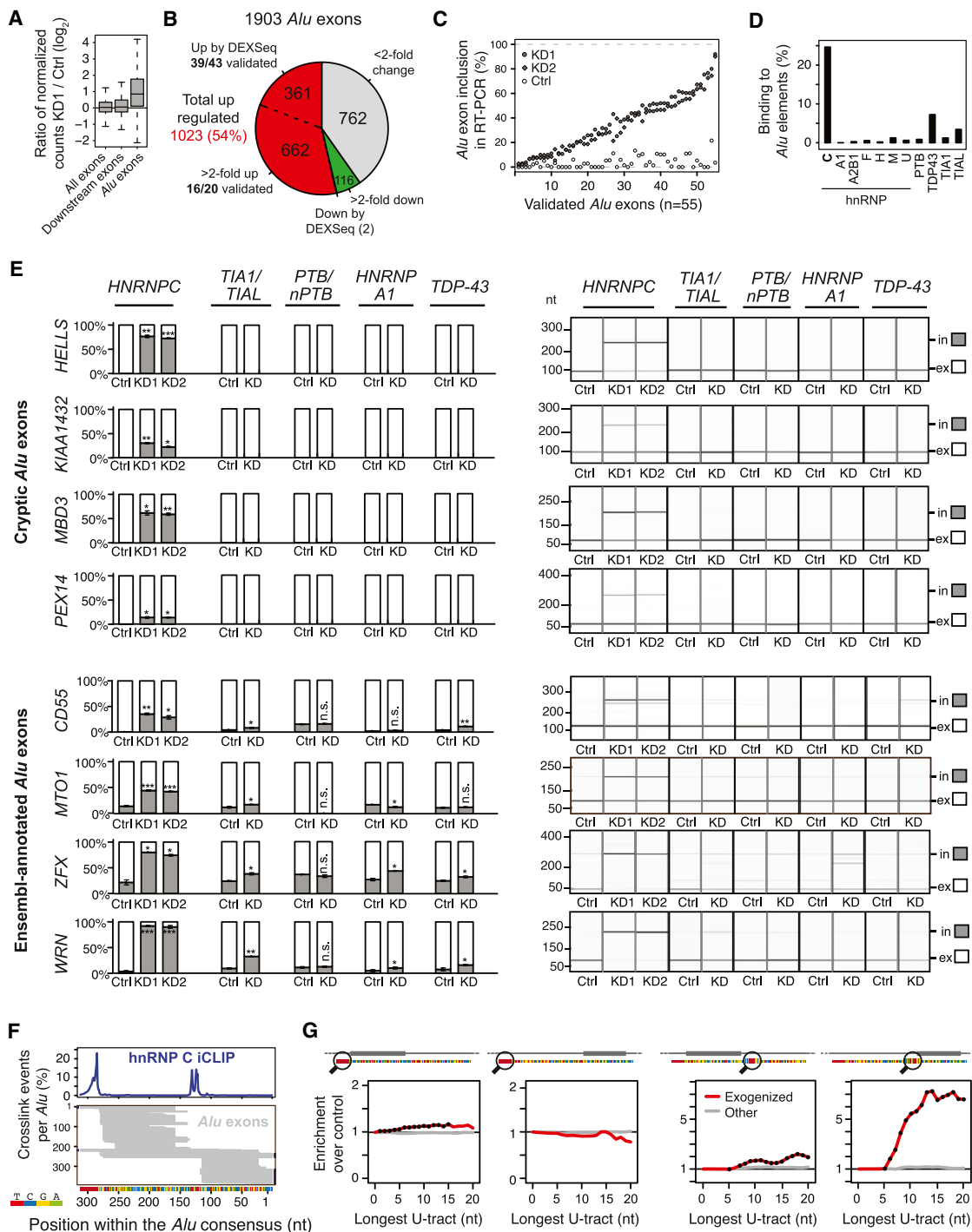


Figure 3. The HNRNPC Knockdown Leads to Widespread Exonization of Antisense *Alu* Elements

(A) Box plots summarizing the change in normalized expression of *Alu* exons compared to downstream non-*Alu* exons as well as all exons.

(B) Pie chart summarizing the regulation of all 1,903 *Alu* exons detect from our RNA-seq data. Upregulated and downregulated exons are further subdivided into those called by DEXSeq or displaying a more than 2-fold change in the HNRNPC knockdown.

(C) Plot depicting the mean inclusion levels in control HeLa cells (open diamonds) and both HNRNPC knockdowns (KD1, filled circles; KD2, filled diamonds) of 55 *Alu* exons that were measured by RT-PCR (Data S1A and S1B).

(D) Bar chart showing the percentage of binding sites of hnRNP C and ten other RNA-binding proteins (indicated below) that overlap with antisense *Alu* elements.

(E) Semiquantitative RT-PCR analyses of four cryptic and four Ensembl-annotated *Alu* exons (indicated on the left) upon knockdown of HNRNPC (two independent knockdowns, KD1 and KD2), TIA1/TIAL, PTB/nPTB, HNRNPA1, and TDP-43 (labeled as KD with the respective gene[s] indicated above) as well as in

(legend continued on next page)

A major source of cryptic exons are *Alu* elements. They are the most abundant transposable elements in the human genome, present in over 50% of all introns (Deininger, 2011). They contain two arms separated by a poly(A) linker sequence and followed by a poly(A) tail. When integrated into genes in the antisense orientation, the poly(A) sequences are transcribed as U-tracts (referred to as the upstream and the linker U-tract) that can serve as polypyrimidine tracts to promote recognition of the cryptic splice sites that exist within the *Alu* elements (Deininger, 2011). During primate evolution, many *Alu* elements evolved into genuine exons in a process called “exonization.” Among them is the Ensembl-annotated *Alu* exon in the *CD55* gene, whose inclusion is clearly regulated via competition between hnRNP C and U2AF65 (Figure 1C).

Our RNA-seq data document the presence of a large number of *Alu*-derived exons. In addition to 585 Ensembl-annotated *Alu* exons, we find 1,318 cryptic exons that originated from *Alu* elements, yielding a total of 1,903 *Alu* exons for further analysis (Table S2). hnRNP C depletion leads to a dramatic global increase in *Alu* exon inclusion (Figures 3A and S4C): we detect a total of 1,023 upregulated *Alu* exons that are either identified by the DEXSeq software (361 exons) or display a more than 2-fold change in at least one knockdown (662 exons; Figures 3B and S4C; Table S2). We used these two thresholds because many *Alu* exons are expressed at low levels, leading to lower statistical power for the DEXSeq analysis.

We confirmed the splicing changes by semiquantitative RT-PCR, validating 39 out of 43 (91%) DEXSeq-called *Alu* exons and 16 out of 20 (80%) *Alu* exons with more than 2-fold change (Figure 3C; Data S1; Table S3). We conclude that more than 1,000 *Alu* exons show a considerable increase in inclusion upon hnRNP C depletion (Figure 3B). Most *Alu* exons are barely detectable in the control samples (Figure 3C), emphasizing how efficiently they are suppressed under normal conditions. In contrast, these same exons display up to 90% inclusion in the knockdown. Together, these results demonstrate that hnRNP C safeguards the transcriptome from aberrant and potentially detrimental expression of cryptic exons, most particularly those originating from *Alu* elements.

Finally, we tested whether the repression of *Alu* exons is specific to hnRNP C. Among ten other RNA-binding proteins tested, TDP-43 and TIAL show most binding to *Alu* elements (7.2% and 3.4% of binding sites, respectively; Figure 3D), but far less than hnRNP C (25%; see below). We also tested the inclusion of four cryptic and four Ensembl-annotated *Alu* exons upon depletion of TDP-43, TIA1/TIAL, as well as hnRNP A1 and PTB/nPTB. None of these knockdowns triggers exonization

of the cryptic *Alu* exons (Figure 3E; Data S1C). For the Ensembl-annotated *Alu* exons, we find some regulation by all proteins. However, all of these changes are small compared to the impact of hnRNP C depletion, and we cannot exclude indirect effects; for instance, *TIA1/TIAL* knockdown was previously described to alter the splicing pattern of *HNRNPC* (Wang et al., 2010). In summary, we conclude that the suppression of *Alu* exons is specifically and primarily achieved by hnRNP C.

The U-Tracts Facilitate Strong hnRNP C Binding to *Alu* Elements

The impact of hnRNP C function extends far beyond the 1,000 *Alu* exons that we detect as repressed by hnRNP C. hnRNP C binds extensively to antisense *Alu* elements in the transcriptome: we detect binding to 72,625 intronic antisense *Alu* elements, comprising 21% of all antisense *Alu* elements in the transcriptome (compared with only 0.03% of sense *Alu* elements). In fact, 25% of all hnRNP-C-binding sites occur within intronic *Alu* elements, underlining that repression of *Alu* exonization is a major role of hnRNP C. Within the *Alu* elements, hnRNP C recognizes the upstream and linker U-tracts, where its binding coincides with cryptic *Alu* exons originating from both arms (Figures 3F, S4D, and S4E). Together, these observations suggest that the long continuous U-tracts of the *Alu* elements attract strong hnRNP C binding and serve as a critical interface to control *Alu* exonization.

We further assessed the importance of the U-tracts in *Alu* elements by performing an evolutionary analysis measuring the strength of selection. Compared with unexonized *Alu* elements, *Alu* elements that give rise to hnRNP-C-repressed exons show a remarkable tendency to preserve and even lengthen U-tracts (Figure 3G). This indicates that stronger hnRNP C binding and hence stronger repression of cryptic *Alu* exons provided a substantial fitness benefit during primate evolution, and that accidental *Alu* exonization imposes a significant cost to survival. In contrast, a separate comparison with 81 established *Alu* exons, which are included in control cells and do not change in the *HNRNPC* knockdown, reveals a trend toward shorter U-tracts and mutations that weaken hnRNP-C-binding (Figures S5A–S5C). These observations indicate that there is overwhelming selection pressure to repress aberrant *Alu* exonization through hnRNP C binding, and that this is relieved in only a very small subset of *Alu* elements that become genuine exons.

The Competition between hnRNP C and U2AF65 Controls *Alu* Exonization

To investigate whether hnRNP C interferes with U2AF65 binding to cryptic exons, we compared binding patterns in the

control HeLa cells (Ctrl). Known target exons of these proteins can be found in Data S1C. (Right) Gel views of capillary electrophoresis of the PCR products with the fragments including (in) or excluding (ex) the *Alu* exon marked on the right. (Left) Bar diagrams depicting the mean inclusion (gray) and exclusion (white) level in each sample. Asterisks indicate the significance level (Student's t test) relative to control: n.s., nonsignificant; *p value < 0.05; **p value < 0.001; ***p value < 0.0001. Error bar represents SDM; n = 3.

(F) Schematic representations of hnRNP C crosslink events per nucleotide (top) and of *Alu* exon locations (bottom) along the *Alu* consensus sequence. Exons that extend beyond the *Alu* element end with a blue dash.

(G) Plots depicting the ratio of the cumulative frequencies of U-tracts of a given length (e.g., at least five uridines) in exonized *Alu* elements (red line) compared to nonexonized *Alu* elements within the same genes. Analyses are separately shown for *Alu* exons from the first or second arm of the *Alu* element (gray rectangle above) as well as for the upstream and linker U-tracts (magnifier icon). Nonexonized *Alu* elements of all other genes (gray line) serve as control. Black dots, p value < 0.05 (Pearson's chi-square test).

See also Figures S4 and S5, Data S1, and Table S3.

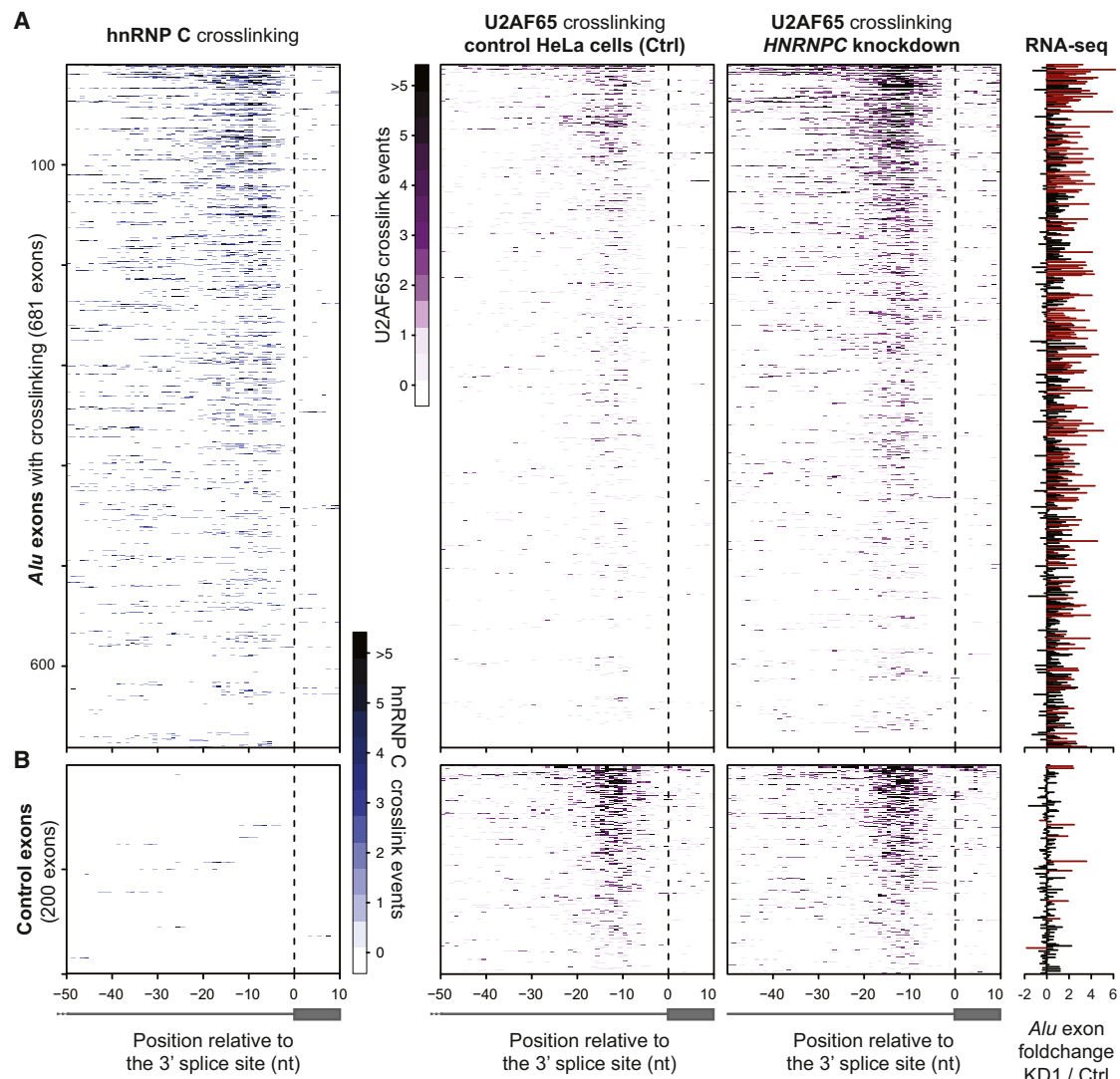


Figure 4. The Competition of hnRNP C with U2AF65 at 3' Splice Sites Represses Alu Exon Inclusion

(A) Heatmaps comparing the amount of crosslinking of hnRNP C (left; different shades of blue) and U2AF65 (different shades of purple) in control (middle) and HNRNPC knockdown cells (right) relative to the 3' splice sites of *Alu* exons (indicated by a dashed line). U2AF65 iCLIP data were corrected for differences in library sizes. Each row corresponds to one of 681 *Alu* exons that contain at least five crosslink events within the analyzed region (from -50 nt to +10 nt relative to the first nucleotide of the exon). The bar diagram on the right shows the fold change in *Alu* exon inclusion (KD1 over wild-type; differentially regulated exons according to conditional thresholding are shown in red).

(B) Heatmaps as in (A) for a subset of 200 control non-*Alu* exons that lie downstream within the same genes (full set in Figure S5D).

See also Figure S5.

knockdown and control samples. We find a 3.3-fold increase in U2AF65 binding at the 3' splice sites of *Alu* exons in the HNRNPC knockdown (Figure 4A). This effect is specific for the *Alu* exons, because downstream control exons remain unaffected (Figures 4B and S5D). This indicates that hnRNP C efficiently blocks U2AF65 from *Alu* elements.

To confirm that the integrity of the U-tract is important for hnRNP-C-based repression of *Alu* exons, we generated a mini-gene containing the Ensembl-annotated *Alu* exon within the *CD55* gene (Figures 1 and 5A). Based on our *in vitro* UV-cross-linking assays, we hypothesized that mutations disrupting the

U-tract but preserving the polypyrimidine tract would weaken hnRNP C binding and hence increase exon inclusion. We find that two point mutations in the upstream U-tract are sufficient to elevate inclusion levels in the presence of hnRNP C (Figure 5), confirming that high-affinity hnRNP C binding is critical for efficient competition with U2AF65. Consistent with our previous observation that hnRNP C binding occurs on both sides of regulated exons (König et al., 2010), introduction of additional mutations in the downstream linker U-tract further increases exon inclusion and almost completely abolishes hnRNP C-dependent regulation.

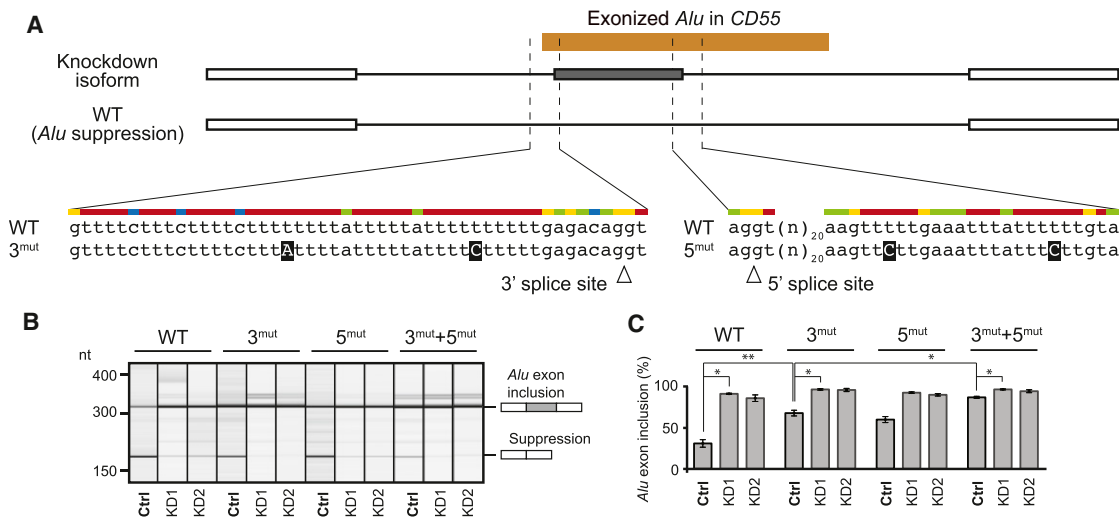


Figure 5. Point Mutations that Impair hnRNP C Binding Promote Inclusion of the *Alu* Exon in the *CD55* Minigene

(A) Schematic overview of the minigene including the *Alu* exon (gray square), intronic regions (black lines), and two flanking exons (white squares) from the *CD55* gene. The original sequence (WT) as well as the mutated sequence surrounding the 3' and 5' splice sites (3^{mut} and 5^{mut}, respectively; splice sites marked by arrowheads) are depicted below. Introduced point mutations are highlighted in black.

(B) RT-PCR monitoring inclusion or suppression of the *Alu* exon in the minigenes with wild-type (WT) or mutated sequences (3^{mut}, 5^{mut}) in *hnRNP C* knockdown (KD1 and KD2) and control HeLa cells (Ctrl). The corresponding capillary electrophoresis data is given in a gel-like representation with *Alu* exon inclusion and suppression indicated schematically on the right.

(C) Average *Alu* exon inclusion in percent from three replicate RT-PCR experiments. Lines indicate relevant comparisons with asterisks representing different levels of significance (*p value < 0.05; **p < 10⁻³; Student's t test). Error bars represent SDM.

See also Figure S6 and Table S5.

To test the effects of similar mutations in cryptic *Alu* exons, we generated another minigene containing the intronic *Alu* element in the *NUP133* gene that exonizes upon *hnRNP C* knockdown (Figure S6A). As observed for *CD55*, introduction of three point mutations in the upstream U-tract is sufficient to promote *Alu* exonization, and two additional mutations in the linker U-tract completely abolish *hnRNP C* repression (Figure S6). In summary, these experiments demonstrate that the competition between *hnRNP C* and *U2AF65* controls *Alu* exonization, and that weakening *hnRNP C* binding is sufficient to promote exon inclusion.

Mutations Disrupting *hnRNP-C*-Dependent Repression of *Alu* Exons Can Cause Disease

Erroneous *Alu* exon inclusion has been implicated in various diseases (Vorechovsky, 2010). For instance, exonization of an intronic *Alu* element in the *PTS* gene has been associated with hyperphenylalaninemia (Meili et al., 2009): deletion of the upstream U-tract leads to *Alu* exon inclusion from a downstream, cytidine-rich polypyrimidine tract. We observe strong *hnRNP C* binding at this U-tract, and exonization of the *Alu* element in the *hnRNP C* knockdown (Figure 6A; Data S1A). We designed a *PTS* minigene to test whether the disease mutation disrupts the ability of *hnRNP C* to repress this *Alu* exon (Figure 6A). As expected, there is almost no *Alu* exon inclusion in the control HeLa cells, while *hnRNP C* knockdown leads to a strong increase in aberrant exonization (Figures 6B and 6C). As previously described (Meili et al., 2009), introduction of the disease-associated mutation increases the aberrant exon inclusion in

the control samples. Importantly, we show that *hnRNP C* depletion does not produce any additional effect (Figures 6B and 6C). This suggests that *hnRNP-C*-dependent repression is completely abolished by the clinically relevant mutation. These experiments demonstrate that *hnRNP C* binding is crucial for preventing the unwanted exonization of this *Alu* element under normal conditions.

We also assessed the broader protective function of *hnRNP C* in maintaining transcriptome integrity. Almost 80% of the *Alu* exons in our RNA-seq data are predicted to introduce frameshifts or stop codons that will strongly impair the function of the 1,572 genes containing them. Once included in processed transcripts, these *Alu* elements are likely to impair the function of the final protein product and could target the respective transcripts into the nonsense-mediated decay pathway (Mendell et al., 2004). In line with *Alu* exon-induced transcript degradation, we observe a correlation between *Alu* exon inclusion and downregulation of the corresponding transcripts in the *hnRNP C* knockdown (Figures 6D and S4F). *hnRNP C*'s importance is further underlined by the observation that the affected transcripts are implicated in a broad range of cellular functions (Table S4). For instance, *hnRNP C* represses *Alu* exons in *BAX*, *VHL*, *RAD52*, and *HELLS*, which encode proteins with key functions during development and disease.

DISCUSSION

A growing catalog of genome-wide CLIP studies continues to generate fascinating insights into the diverse functions of

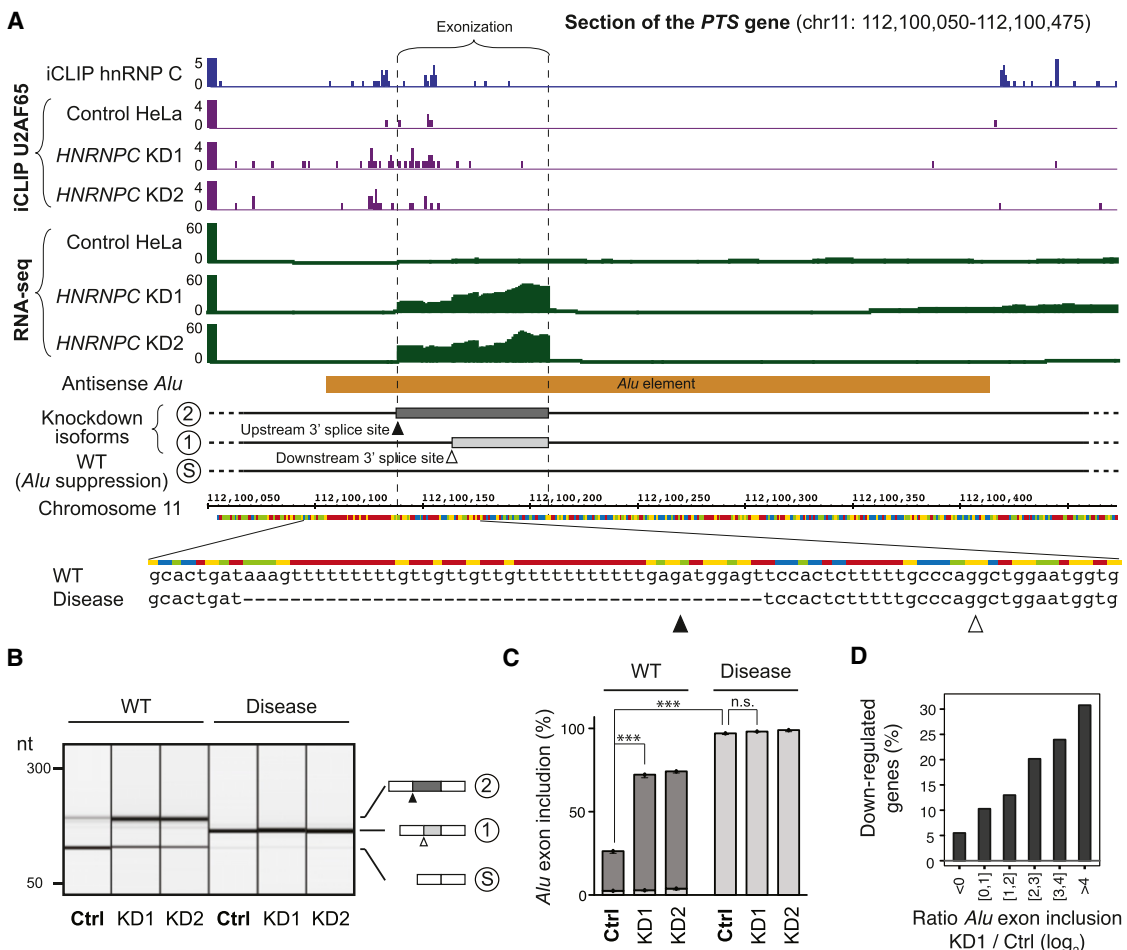


Figure 6. hnRNP C Repression of Alu Exonization in the PTS Gene Is Relevant for Disease

(A) Genome browser view including the disease-relevant *Alu* element (orange) within the *PTS* gene. iCLIP data for hnRNP C (blue) and U2AF65 (purple) from *HNRRNP*C knockdown (KD1 and KD2) and control HeLa cells as well as RNA-seq data (green) are shown above. The corresponding isoforms are schematically indicated: *Alu* suppression in isoform S, usage of the downstream 3' splice site (open arrowhead) in isoform 1 (light gray; this isoform is produced as a result of the disease-associated deletion which removes the upstream 3' splice site together with the U-tract) and usage of the upstream 3' splice site (filled arrowhead) in isoform 2. Wild-type sequence (WT) and disease-associated deletion are shown below.

(B) Gel-like view of capillary electrophoresis of RT-PCR analyses of minigenes containing the *Alu* element described in (A) with the two flanking exons. The different isoforms are schematically indicated on the right.

(C) Average *Alu* exon inclusion in percent from three replicate RT-PCR experiments. Lines indicate relevant comparisons with asterisks representing different levels of significance (**p < 10⁻⁴; n.s., not significant; Student's t test). Error bars represent SDM.

(D) Bar diagram depicting the fraction of downregulated genes within sets of genes carrying *Alu* exons with different levels of upregulation in KD1 (intervals of the fold change in inclusion in KD1 are given below).

See also Table S5.

RNA-binding proteins. Combining these data with additional functional information allows us to interpret the consequences of RNA binding in diverse cellular processes, including alternative splicing, 3' end processing, and translation (Darnell et al., 2011; Hafner et al., 2010; König et al., 2010, 2012; Licatalosi et al., 2008; Ule et al., 2003; Wang et al., 2012).

In this study, we developed the iCLIP approach a step further: the refined technique allowed us not only to discover many protein-RNA interactions, but also to quantify the relative strengths of these associations under different conditions. This enabled the quantitative measurement of competitive binding

between two RNA-binding proteins on a transcriptome-wide scale. Specifically, our study combines experimental and computational genomic approaches to describe a general mechanism for regulating splicing via competitive RNA binding, uncover a safeguarding mechanism for transcriptome integrity, and provide insights into *Alu*-derived exon evolution.

How Competitive Binding Determines the Splicing Outcome

Many splicing decisions are made in the early phases of spliceosome assembly (Wahl et al., 2009). An important checkpoint is

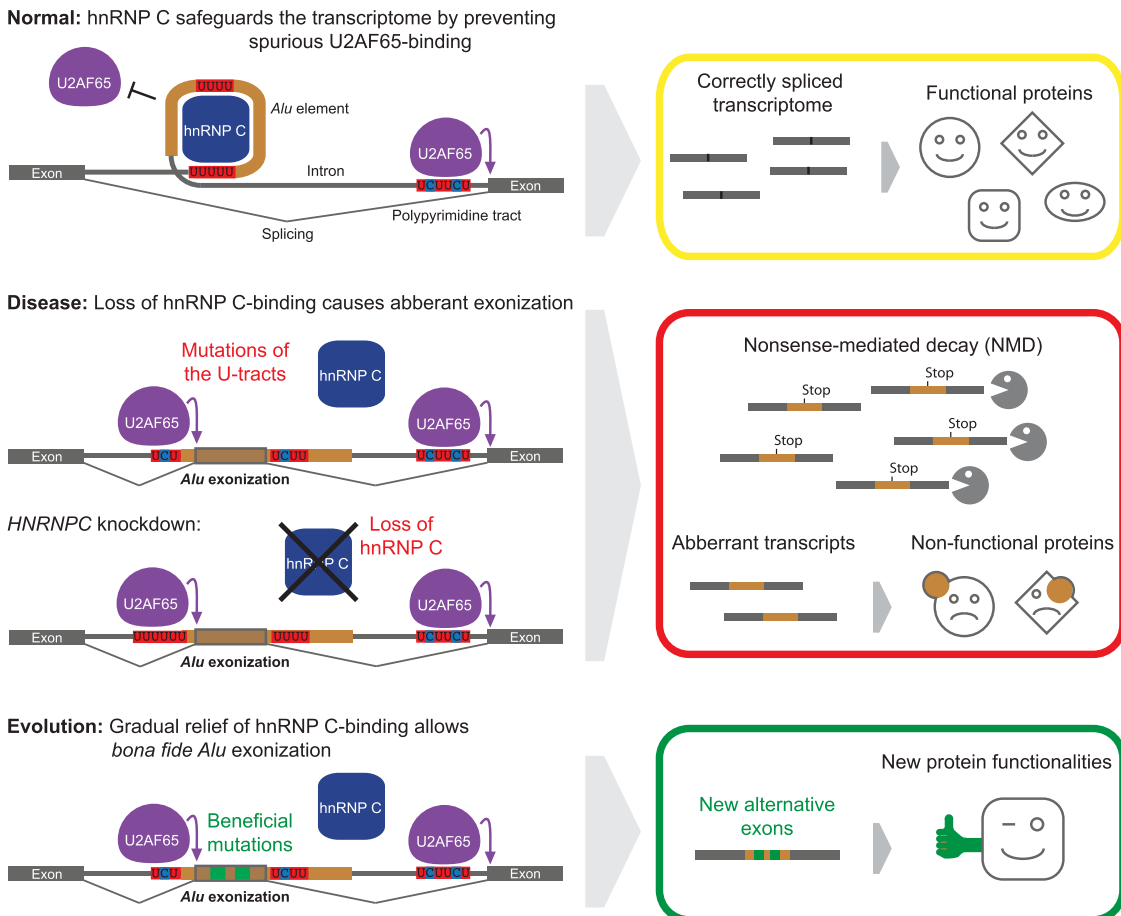


Figure 7. hnRNP C Safeguards the Transcriptome from the Exonization of *Alu* Elements

In normal cells, hnRNP C prevents recognition of the *Alu* elements through U2AF65, thereby ensuring accurate splicing. In the *HNRNPC* knockdown, U2AF65 can bind to the U-tracts and promote *Alu* exonization. Similarly, disease-associated mutations in the U-tracts can favor *Alu* exonization in the presence of hnRNP C by impairing hnRNP-C-binding. The resulting nonfunctional transcripts are likely either targeted by nonsense-mediated decay (NMD) or give rise to nonfunctional proteins. Once an exon acquires beneficial changes during evolution, similar mutations accumulate to relieve hnRNP C repression, opening the possibility for new protein functionalities.

the binding of U2AF65 to the polypyrimidine tract, which is targeted by multiple regulators (Wahl et al., 2009). U2AF65 has a broad binding specificity for motifs comprising both uridines and cytidines, leading to recognition of a very heterogeneous spectrum of polypyrimidine tracts (Singh et al., 2000). hnRNP C's comparatively strict specificity for U-tracts allows hnRNP C to selectively compete with U2AF65 on a subset of sites, most prominently at cryptic splice sites within *Alu* elements (see below). U2AF65's degenerate specificity also opens the possibility of competitive binding with other regulators at defined subsets of sites. Accordingly, many splicing factors apart from hnRNP C are recruited to specific sets of polypyrimidine tracts to regulate downstream exons (Licatalosi et al., 2008; Llorian et al., 2010; Wang et al., 2012; Xue et al., 2009), and some of these were shown to modulate U2AF65 binding. For instance, competitive binding by PTB to the β -tropomyosin transcript is associated with reduced U2AF65 binding and decreased exon 6 inclusion (Saulière et al., 2006). Similarly, hnRNP A/B proteins

prevent U2AF65 binding to an alternative splice site in HIV-1 pre-mRNA by polymerizing across the polypyrimidine tract (Domsic et al., 2003). These observations underline the crucial role of the polypyrimidine tract as a regulatory hub, which enables the interplay of multiple regulators with the splicing machinery.

hnRNP C Prevents Spurious U2AF65 Recognition of Cryptic Splice Sites

Perhaps the most striking result of the study is that hnRNP C binds to more than 70,000 *Alu* elements, and that the absence of hnRNP C gives rise to more than a thousand cryptic *Alu* exons. hnRNP C prevents exonization of the *Alu* elements by strongly binding to their U-tracts. Indeed, our minigene experiments suggest that hnRNP C's competition with U2AF65 at U-tracts upstream of 3' splice sites constitutes a major mechanism of *Alu* exon repression (Figure 7). In addition to the effect at 3' splice sites, we also detected hnRNP C binding to U-tracts downstream of 5' splice sites. Here, hnRNP C might interfere with

binding of TIA1 and TIAL, which were previously described to enhance 5' splice-site usage in *Alu* exons (Förch et al., 2002; Gal-Mark et al., 2009). In addition, simultaneous binding to both U-tracts might aid the formation of stable hnRNP particles (Huang et al., 1994; König et al., 2010), which would in turn reinforce hnRNP C's capacity to compete with U2AF65 and other splicing factors.

Alu exon repression is specific for hnRNP C. In particular, we could exclude an involvement of hnRNP A1, which was previously shown to proofread U2AF binding (Tavanez et al., 2012). This is not unexpected, because hnRNP A1 proofreading relies on the absence of an AG dinucleotide in the 3' splice site, which is commonly present downstream of U-tracts in *Alu* elements. Similarly, depletion of other regulators like TIA1, TIAL, TDP-43, and PTB did not trigger the inclusion of cryptic *Alu* exons.

Deleterious Consequences of Aberrant *Alu* Exonization in the Absence of hnRNP C

The increasing number of reported *Alu*-associated disorders illustrates that the enormous amounts of *Alu* elements pose a serious threat to the normal function of human cells (Hedges and Deininger, 2007; Krehling and Graveley, 2004). Diseases like congenital cataracts, facial dysmorphism, neuropathy syndrome are caused by the inclusion of intronic *Alu* elements that severely disrupt the transcript structure, thereby affecting the function of the resulting protein (Varon et al., 2003). Indeed, a recent study estimated that 11 of 78 documented genetic diseases involving cryptic exons are associated with mutations in *Alu* elements (Vorechovsky, 2010). Although some studies have previously suggested the involvement of *trans*-acting factors (Lin et al., 2009; Shen et al., 2011; Sorek et al., 2002), the mechanisms by which cells protect against spurious exonization of *Alu* elements has remained unknown until now.

Our study establishes that one of hnRNP C's principal functions is to protect the human transcriptome from aberrant *Alu* exonization. It is important to note that our current analysis of 2,000 *Alu* exons most likely underestimates the full scale of aberrant exonization in the absence of hnRNP C; this is because *Alu* elements are notoriously difficult to detect by current RNA-seq methods (Treangen and Salzberg, 2012). Furthermore, although the present study focuses on *Alu* elements because they represent the largest family of retrotransposons in the human genome, we suggest that hnRNP C might be important for suppressing retrotransposon-derived exons in general. Their poly(A) tails, and hence U-tracts when in antisense orientation, are required for efficient retrotransposition (Deininger, 2011; Dewannieux et al., 2003). In summary, we propose that hnRNP C plays a critical role in preserving human health by safeguarding transcriptome integrity against the detrimental effects of spurious exonization.

hnRNP-C-Mediated Repression May Also Facilitate Evolutionary Innovation

More than 650,000 *Alu* elements reside within the transcribed regions of the human genome. Although we have stressed the threat posed by the loss of hnRNP C repression, many studies have highlighted the potential for *Alu* exonization to introduce genomic variation and evolutionary innovations (Häsler et al.,

2007; Lev-Maor et al., 2003; Schmitz and Brosius, 2011; Shen et al., 2011). A well-studied example is the inclusion of the *Alu* exon in the *CD55* gene, which is regulated by hnRNP C and converts the encoded protein from a membrane-bound to a secreted version (Caras et al., 1987). Genuine *Alu*-derived exons are estimated to contribute 5% of all internal alternative exons: they are particularly enriched among recently acquired exons (Sela et al., 2007; Sorek, 2007; Vorechovsky, 2010) and are present in half of the human-specific genes, underlining their likely involvement in genome evolution and species-specific adaptation (Keren et al., 2010; Shen et al., 2011; Toll-Riera et al., 2009).

While the evolutionary potential of *Alu* exonization has attracted considerable interest (Sorek, 2007), the sudden incorporation of *Alu* elements into mature transcripts is likely to be deleterious in the vast majority of cases. In this context, the role of hnRNP C as a global suppressor may have important implications for evolutionary adaptation: in the presence of hnRNP C, *Alu* elements are repressed instead of being removed from the genome through selection, allowing them to evolve near-neutrally for longer evolutionary times. Cryptic *Alu* exons that are deleterious will remain suppressed; however if an exon becomes less deleterious by chance, selection against exonization will be considerably reduced. Mutations to the U-tracts that change the balance of binding between hnRNP C and splicing factors may allow low levels of "leaky" exonization, which allows even stronger evolutionary testing by selection. This could also be achieved by recruitment of additional factors that stabilize spliceosome binding and counteract hnRNP C interference, thereby circumventing the need to completely remove long U-tracts. Sequential mutations would thus enable an incremental exonization process, which could eventually lead to loss of hnRNP-C-dependent repression if an exon becomes functional and provides adaptive potential (Figure 7).

In conclusion, we propose that hnRNP C plays a critical role in protecting the transcriptome from the harmful effects of aberrant *Alu* exonization, while stabilizing a large reservoir of *Alu* elements in the human genome to facilitate the evolutionary exploration of new functions. The hnRNP-C-mediated regulation of *Alu* exonization has important implications for the evolution of the human genome and disease progression.

EXPERIMENTAL PROCEDURES

RNA-Seq Analyses

RNA-seq libraries were sequenced on an Illumina GA-2 (72 cycles, paired end) and mapped to the human genome hg19 using TopHat (Trapnell et al., 2009; Table S1).

iCLIP Experiments

iCLIP experiments were performed as described in König et al. (2011) using monoclonal mouse antibody (4F4) from Santa Cruz (sc-32308) for hnRNP C and a monoclonal mouse antibody (MC3) from Sigma (U4758) for U2AF65 (Tables S1 and S5). A summary of major steps can be found in the legends of Figures S2A and S2B.

HNRNPC Knockdown

Knockdown of *HNRNPC* in HeLa cells was achieved with hnRNP C Stealth Select RNAi siRNAs HSS179304 and HSS179305 as well as control siRNA Stealth RNAi siRNA Negative Control (Invitrogen).

Expression of Recombinant Proteins

Recombinant glutathione S transferase (GST)-tagged full-length hnRNP C1 and His-tagged U2AF65^{RRM12} comprising residues 148–342 were purified from *Escherichia coli* BL21-CodonPlus(DE3)-RP cells (Stratagene).

De Novo Exon Prediction and Classification

Exon coordinates were predicted using Cufflinks (Trapnell et al., 2010) followed by several quality filters (Table S2). *Alu* exons were defined as exons with at least one splice site within an antisense *Alu* element (taken from RepBase; Jurka et al., 2005) that was supported by at least one junction-spanning read.

Calculation of RBP Occupancy and Differential Binding

To correct RBP occupancy for changes in gene expression, we normalized each binding site to the total amount of crosslinking within the respective gene. Differential binding of U2AF65 was assessed using the \log_2 -transformed ratio of normalized occupancies (KD/Ctrl). To allow direct comparison of U2AF65 binding from *HNRNPC* knockdown and control samples, we corrected the occupancies for the different iCLIP library sizes using DESeq (Anders and Huber, 2010).

Further experimental and computational methods are described in Extended Experimental Procedures.

ACCESSION NUMBERS

The ArrayExpress accession numbers for the RNA-seq and iCLIP data are E-MTAB-1147 and E-MTAB-1371, respectively.

SUPPLEMENTAL INFORMATION

Supplemental Information includes Extended Experimental Procedures, six figures, five tables, and one data file and can be found with this article online at <http://dx.doi.org/10.1016/j.cell.2012.12.023>.

ACKNOWLEDGMENTS

The authors thank all members of the Ule and Luscombe laboratories for assistance and discussion, in particular Zhen Wang and Miha Modic for sharing RNA samples from *TIA1/TIAL* and *TDP-43* knockdown cells. We thank Tomaž Cerk, Gregor Rot, and Črt Gorup for their work on the iCount pipeline, as well as James Hadfield for high-throughput sequencing. We are grateful for materials, data, and advice provided by Chris Smith, Miguel Coelho, Miriam Lorian, Wing-Fung (Wilfred) Wu, Michael Sattler, Yun Zhang, Frédéric Allain, Zuzana Cienikova, Gene Yeo, Stephanie Huelga, Gil Ast, Galit Lev-Maor, Noa Sela, Juan Valcárcel, Joao Tavanez, and Gautier Koscielny. This work was supported by the European Research Council (grant 206726-CLIP) and the Medical Research Council (grant U105185858) (to J.U.), an EMBL EIPOD fellowship (to K.Z.), and a Long-term Human Frontiers Science Program fellowship (to J.K.).

Received: May 25, 2012

Revised: September 22, 2012

Accepted: December 12, 2012

Published: January 31, 2013

REFERENCES

Anders, S., and Huber, W. (2010). Differential expression analysis for sequence count data. *Genome Biol.* 11, R106.

Anders, S., Reyes, A., and Huber, W. (2012). Detecting differential usage of exons from RNA-seq data. *Genome Res.* 22, 2008–2017. <http://dx.doi.org/10.1101/gr.133744.133111>.

Beyer, A.L., Christensen, M.E., Walker, B.W., and LeStourgeon, W.M. (1977). Identification and characterization of the packaging proteins of core 40S hnRNP particles. *Cell* 11, 127–138.

Buratti, E., Chivers, M., Královicová, J., Romano, M., Baralle, M., Krainer, A.R., and Vorechovsky, I. (2007). Aberrant 5' splice sites in human disease genes: mutation pattern, nucleotide structure and comparison of computational tools that predict their utilization. *Nucleic Acids Res.* 35, 4250–4263.

Caras, I.W., Davitz, M.A., Rhee, L., Weddell, G., Martin, D.W., Jr., and Nusenzweig, V. (1987). Cloning of decay-accelerating factor suggests novel use of splicing to generate two proteins. *Nature* 325, 545–549.

Choi, Y.D., Grabowski, P.J., Sharp, P.A., and Dreyfuss, G. (1986). Heterogeneous nuclear ribonucleoproteins: role in RNA splicing. *Science* 231, 1534–1539.

Darnell, J.C., Van Driesche, S.J., Zhang, C., Hung, K.Y., Mele, A., Fraser, C.E., Stone, E.F., Chen, C., Fak, J.J., Chi, S.W., et al. (2011). FMRP stalls ribosomal translocation on mRNAs linked to synaptic function and autism. *Cell* 146, 247–261.

Deininger, P. (2011). *Alu* elements: know the SINEs. *Genome Biol.* 12, 236.

Dewannieux, M., Esnault, C., and Heidmann, T. (2003). LINE-mediated retrotransposition of marked *Alu* sequences. *Nat. Genet.* 35, 41–48.

Dhir, A., and Buratti, E. (2010). Alternative splicing: role of pseudoexons in human disease and potential therapeutic strategies. *FEBS J.* 277, 841–855.

Domsic, J.K., Wang, Y., Mayeda, A., Krainer, A.R., and Stoltzfus, C.M. (2003). Human immunodeficiency virus type 1 hnRNP A/B-dependent exonic splicing silencer ESSV antagonizes binding of U2AF65 to viral polypyrimidine tracts. *Mol. Cell. Biol.* 23, 8762–8772.

Dreyfuss, G., Matunis, M.J., Piñol-Roma, S., and Burd, C.G. (1993). hnRNP proteins and the biogenesis of mRNA. *Annu. Rev. Biochem.* 62, 289–321.

Fedorova, L., and Fedorov, A. (2003). Introns in gene evolution. *Genetica* 118, 123–131.

Förch, P., Puig, O., Martínez, C., Séraphin, B., and Valcárcel, J. (2002). The splicing regulator TIA-1 interacts with U1-C to promote U1 snRNP recruitment to 5' splice sites. *EMBO J.* 21, 6882–6892.

Gal-Mark, N., Schwartz, S., Ram, O., Eyras, E., and Ast, G. (2009). The pivotal roles of TIA proteins in 5' splice-site selection of *alu* exons and across evolution. *PLoS Genet.* 5, e1000717.

Görlach, M., Burd, C.G., and Dreyfuss, G. (1994). The determinants of RNA-binding specificity of the heterogeneous nuclear ribonucleoprotein C proteins. *J. Biol. Chem.* 269, 23074–23078.

Hafner, M., Landthaler, M., Burger, L., Khorshid, M., Hausser, J., Berninger, P., Rothbächer, A., Ascano, M., Jr., Jungkamp, A.C., Munschauer, M., et al. (2010). Transcriptome-wide identification of RNA-binding protein and microRNA target sites by PAR-CLIP. *Cell* 141, 129–141.

Häslar, J., Samuelsson, T., and Strub, K. (2007). Useful ‘junk’: *Alu* RNAs in the human transcriptome. *Cell. Mol. Life Sci.* 64, 1793–1800.

Hedges, D.J., and Deininger, P.L. (2007). Inviting instability: Transposable elements, double-strand breaks, and the maintenance of genome integrity. *Mutat. Res.* 616, 46–59.

Heiner, M., Hui, J., Schreiner, S., Hung, L.H., and Bindereif, A. (2010). HnRNP L-mediated regulation of mammalian alternative splicing by interference with splice site recognition. *RNA Biol.* 7, 56–64.

Huang, M., Rech, J.E., Northington, S.J., Flicker, P.F., Mayeda, A., Krainer, A.R., and LeStourgeon, W.M. (1994). The C-protein tetramer binds 230 to 240 nucleotides of pre-mRNA and nucleates the assembly of 40S heterogeneous nuclear ribonucleoprotein particles. *Mol. Cell. Biol.* 14, 518–533.

Huelga, S.C., Vu, A.Q., Arnold, J.D., Liang, T.Y., Liu, P.P., Yan, B.Y., Donohue, J.P., Shiue, L., Hoon, S., Brenner, S., et al. (2012). Integrative genome-wide analysis reveals cooperative regulation of alternative splicing by hnRNP proteins. *Cell Rep.* 1, 167–178.

Jurka, J., Kapitonov, V.V., Pavlicek, A., Klonowski, P., Kohany, O., and Walichiewicz, J. (2005). Repbase Update, a database of eukaryotic repetitive elements. *Cytogenet. Genome Res.* 110, 462–467.

Keren, H., Lev-Maor, G., and Ast, G. (2010). Alternative splicing and evolution: diversification, exon definition and function. *Nat. Rev. Genet.* 11, 345–355.

König, J., Zarnack, K., Rot, G., Curk, T., Kayikci, M., Zupan, B., Turner, D.J., Luscombe, N.M., and Ule, J. (2010). iCLIP reveals the function of hnRNP particles in splicing at individual nucleotide resolution. *Nat. Struct. Mol. Biol.* 17, 909–915.

König, J., Zarnack, K., Rot, G., Curk, T., Kayikci, M., Zupan, B., Turner, D.J., Luscombe, N.M., and Ule, J. (2011). iCLIP—transcriptome-wide mapping of protein-RNA interactions with individual nucleotide resolution. *J. Vis. Exp.* (50). <http://dx.doi.org/10.3791/2638>.

König, J., Zarnack, K., Luscombe, N.M., and Ule, J. (2012). Protein-RNA interactions: new genomic technologies and perspectives. *Nat. Rev. Genet.* 13, 77–83.

Kreahling, J., and Graveley, B.R. (2004). The origins and implications of alternative splicing. *Trends Genet.* 20, 1–4.

Lev-Maor, G., Sorek, R., Shomron, N., and Ast, G. (2003). The birth of an alternatively spliced exon: 3' splice-site selection in *Alu* exons. *Science* 300, 1288–1291.

Licatalosi, D.D., Mele, A., Fak, J.J., Ule, J., Kayikci, M., Chi, S.W., Clark, T.A., Schweitzer, A.C., Blume, J.E., Wang, X., et al. (2008). HITS-CLIP yields genome-wide insights into brain alternative RNA processing. *Nature* 456, 464–469.

Lin, L., Jiang, P., Shen, S., Sato, S., Davidson, B.L., and Xing, Y. (2009). Large-scale analysis of exonized mammalian-wide interspersed repeats in primate genomes. *Hum. Mol. Genet.* 18, 2204–2214.

Llorian, M., Schwartz, S., Clark, T.A., Hollander, D., Tan, L.Y., Spellman, R., Gordon, A., Schweitzer, A.C., de la Grange, P., Ast, G., and Smith, C.W. (2010). Position-dependent alternative splicing activity revealed by global profiling of alternative splicing events regulated by PTB. *Nat. Struct. Mol. Biol.* 17, 1114–1123.

Mackereth, C.D., Madl, T., Bonnal, S., Simon, B., Zanier, K., Gasch, A., Rybin, V., Valcárcel, J., and Sattler, M. (2011). Multi-domain conformational selection underlies pre-mRNA splicing regulation by U2AF. *Nature* 475, 408–411.

Meili, D., Kralovicova, J., Zagalak, J., Bonafé, L., Fiori, L., Blau, N., Thöny, B., and Vorechovsky, I. (2009). Disease-causing mutations improving the branch site and polypyrimidine tract: pseudoexon activation of LINE-2 and antisense *Alu* lacking the poly(T)-tail. *Hum. Mutat.* 30, 823–831.

Mendell, J.T., Sharifi, N.A., Meyers, J.L., Martinez-Murillo, F., and Dietz, H.C. (2004). Nonsense surveillance regulates expression of diverse classes of mammalian transcripts and mutes genomic noise. *Nat. Genet.* 36, 1073–1078.

Nilsen, T.W., and Graveley, B.R. (2010). Expansion of the eukaryotic proteome by alternative splicing. *Nature* 463, 457–463.

Norton, P.A. (1994). Polypyrimidine tract sequences direct selection of alternative branch sites and influence protein binding. *Nucleic Acids Res.* 22, 3854–3860.

Saulière, J., Sureau, A., Expert-Bezançon, A., and Marie, J. (2006). The polypyrimidine tract binding protein (PTB) represses splicing of exon 6B from the *beta-tropomyosin* pre-mRNA by directly interfering with the binding of the U2AF65 subunit. *Mol. Cell. Biol.* 26, 8755–8769.

Schmitz, J., and Brosius, J. (2011). Exonization of transposed elements: A challenge and opportunity for evolution. *Biochimie* 93, 1928–1934.

Sela, N., Mersch, B., Gal-Mark, N., Lev-Maor, G., Hotz-Wagenblatt, A., and Ast, G. (2007). Comparative analysis of transposed element insertion within human and mouse genomes reveals *Alu*'s unique role in shaping the human transcriptome. *Genome Biol.* 8, R127.

Shen, S., Lin, L., Cai, J.J., Jiang, P., Kenkel, E.J., Stroik, M.R., Sato, S., Davidson, B.L., and Xing, Y. (2011). Widespread establishment and regulatory impact of *Alu* exons in human genes. *Proc. Natl. Acad. Sci. USA* 108, 2837–2842.

Singh, R., Banerjee, H., and Green, M.R. (2000). Differential recognition of the polypyrimidine-tract by the general splicing factor U2AF65 and the splicing repressor sex-lethal. *RNA* 6, 901–911.

Sorek, R. (2007). The birth of new exons: mechanisms and evolutionary consequences. *RNA* 13, 1603–1608.

Sorek, R., Ast, G., and Graur, D. (2002). *Alu*-containing exons are alternatively spliced. *Genome Res.* 12, 1060–1067.

Swanson, M.S., and Dreyfuss, G. (1988). Classification and purification of proteins of heterogeneous nuclear ribonucleoprotein particles by RNA-binding specificities. *Mol. Cell. Biol.* 8, 2237–2241.

Tavanez, J.P., Madl, T., Kooshapur, H., Sattler, M., and Valcárcel, J. (2012). hnRNP A1 proofreads 3' splice site recognition by U2AF. *Mol. Cell* 45, 314–329.

Toll-Riera, M., Bosch, N., Bellora, N., Castelo, R., Armengol, L., Estivill, X., and Albà, M.M. (2009). Origin of primate orphan genes: a comparative genomics approach. *Mol. Biol. Evol.* 26, 603–612.

Tollervey, J.R., Curk, T., Rogelj, B., Briese, M., Cereda, M., Kayikci, M., König, J., Hortobágyi, T., Nishimura, A.L., Zupunski, V., et al. (2011). Characterizing the RNA targets and position-dependent splicing regulation by TDP-43. *Nat. Neurosci.* 14, 452–458.

Trapnell, C., Pachter, L., and Salzberg, S.L. (2009). TopHat: discovering splice junctions with RNA-Seq. *Bioinformatics* 25, 1105–1111.

Trapnell, C., Williams, B.A., Pertea, G., Mortazavi, A., Kwan, G., van Baren, M.J., Salzberg, S.L., Wold, B.J., and Pachter, L. (2010). Transcript assembly and quantification by RNA-Seq reveals unannotated transcripts and isoform switching during cell differentiation. *Nat. Biotechnol.* 28, 511–515.

Treangen, T.J., and Salzberg, S.L. (2012). Repetitive DNA and next-generation sequencing: computational challenges and solutions. *Nat. Rev. Genet.* 13, 36–46.

Ule, J., Jensen, K.B., Ruggiu, M., Mele, A., Ule, A., and Darnell, R.B. (2003). CLIP identifies Nova-regulated RNA networks in the brain. *Science* 302, 1212–1215.

Varon, R., Gooding, R., Steglich, C., Marns, L., Tang, H., Angelicheva, D., Yong, K.K., Ambrugger, P., Reinhold, A., Morar, B., et al. (2003). Partial deficiency of the C-terminal-domain phosphatase of RNA polymerase II is associated with congenital cataracts facial dysmorphism neuropathy syndrome. *Nat. Genet.* 35, 185–189.

Vorechovsky, I. (2006). Aberrant 3' splice sites in human disease genes: mutation pattern, nucleotide structure and comparison of computational tools that predict their utilization. *Nucleic Acids Res.* 34, 4630–4641.

Vorechovsky, I. (2010). Transposable elements in disease-associated cryptic exons. *Hum. Genet.* 127, 135–154.

Wahl, M.C., Will, C.L., and Lührmann, R. (2009). The spliceosome: design principles of a dynamic RNP machine. *Cell* 136, 701–718.

Wang, E.T., Cody, N.A., Jog, S., Biancolella, M., Wang, T.T., Treacy, D.J., Luo, S., Schroth, G.P., Housman, D.E., Reddy, S., et al. (2012). Transcriptome-wide regulation of pre-mRNA splicing and mRNA localization by muscleblind proteins. *Cell* 150, 710–724.

Wang, Z., Kayikci, M., Briese, M., Zarnack, K., Luscombe, N.M., Rot, G., Zupan, B., Curk, T., and Ule, J. (2010). iCLIP predicts the dual splicing effects of TIA-RNA interactions. *PLoS Biol.* 8, e1000530.

Warf, M.B., Diegel, J.V., von Hippel, P.H., and Berglund, J.A. (2009). The protein factors MBNL1 and U2AF65 bind alternative RNA structures to regulate splicing. *Proc. Natl. Acad. Sci. USA* 106, 9203–9208.

Xing, Y., and Lee, C. (2006). Alternative splicing and RNA selection pressure—evolutionary consequences for eukaryotic genomes. *Nat. Rev. Genet.* 7, 499–509.

Xue, Y., Zhou, Y., Wu, T., Zhu, T., Ji, X., Kwon, Y.S., Zhang, C., Yeo, G., Black, D.L., Sun, H., et al. (2009). Genome-wide analysis of PTB-RNA interactions reveals a strategy used by the general splicing repressor to modulate exon inclusion or skipping. *Mol. Cell* 36, 996–1006.